

Optical Engineering

SPIDigitalLibrary.org/oe

Numerical validation of the generalized Harvey–Shack surface scatter theory

Narak Choi
James E. Harvey

Numerical validation of the generalized Harvey–Shack surface scatter theory

Narak Choi

University of Central Florida
Center for Research and Education in Optics and Lasers
The College of Optics and Photonics
Orlando, Florida 32816

James E. Harvey

Photon Engineering LLC
440 S. Williams Boulevard, Suite 106
Tucson, Arizona 85711
E-mail: jimh@photonengr.com

Abstract. The generalized Harvey–Shack (GHS) surface scatter theory is numerically compared to the classical small perturbation method, the Kirchhoff approximation method, and the rigorous method of moments for one-dimensional ideally conducting surfaces whose surface power spectral density function is Gaussian or exhibits an inverse power law (fractal) behavior. In spite of its simple analytic form, our numerical comparison shows that the new GHS theory is valid (with reasonable accuracy) over a broader range of surface parameter space than either of the two classical surface scatter theories. © The Authors. Published by SPIE under a Creative Commons Attribution 3.0 Unported License. Distribution or reproduction of this work in whole or in part requires full attribution of the original publication, including its DOI. [DOI: [10.1117/1.OE.52.11.115103](https://doi.org/10.1117/1.OE.52.11.115103)]

Subject terms: surface scatter theory; scattering from rough surfaces; generalized Harvey–Shack; surface scatter theory; optical surface characterization.

Paper 130719P received May 15, 2013; revised manuscript received Sep. 30, 2013; accepted for publication Oct. 10, 2013; published online Nov. 26, 2013.

1 Introduction

Surface scatter phenomena is an important issue in diverse areas of science and engineering. Predicting the scattered light distribution from a randomly rough surface has been investigated by numerous researchers over the past century. Elfouhaily and Guerin conducted an exhaustive survey in 2004, including 260 references.¹ Many approximate scattering methods were reviewed and it is claimed that each method has advantages for specific applications under certain situations. However, the most widely used methods to predict surface scatter phenomena are the small perturbation method (SPM) and the Kirchhoff approximation (KA) method that were established over 40 years ago as the classical Rayleigh–Rice surface scatter theory² and the Beckmann–Kirchhoff surface scatter theory,³ respectively. The SPM has an explicit smooth surface approximation, but it is accurate for large incident and scattered angles. The KA method is valid for rougher surfaces but exhibits a paraxial limitation imposed by a tangential plane approximation. These two approximate theories are thus complementary, but not all-inclusive, i.e., neither of them, nor the combination of them, adequately describes scattered light behavior for moderately rough surfaces at large incident and/or scattered angles.

Recently, Krywonos et al. described a linear systems formulation of surface scatter theory,⁴ based upon a nonparaxial scalar diffraction analysis.^{5,6} This generalized Harvey–Shack (GHS) surface scatter theory provides insight and understanding not readily gleaned from the two previous theories, and Ref. 4 claims that it provides accurate results for moderately rough surfaces at arbitrary incident and scattered angles. The purpose of the current paper is to provide a rigorous validation of the GHS surface scatter theory and to quantitatively compare its performance to that of the classical Rayleigh–Rice and Beckmann–Kirchhoff theories over the entire domain of relevant surface parameters.

The growing memory capacity and increasing speed of computers has resulted in recent advances in numerical

simulation methods for rough surface scattering that are fast, efficient, and numerically stable.⁷ The method of moments (MoM) using a numerical Monte Carlo calculation for discretizing the integral equation has been implemented and applied to surface scatter analysis in this paper.^{7,8} The integral equation upon which the numerical method is based is exact; however, applying it to real-world scattering problems with the desired accuracy is somewhat restricted because it requires extensive computer resources and long calculation times.

It is reasonable to use the MoM to verify or obtain the region of validity of approximate scattering theories for ideal cases, then apply simple and easy-to-handle approximate methods to real-world scattering problems for situations where the approximate methods are validated to be accurate.^{9–22} Several previous researchers have reported the valid domain of the SPM, KA, and other scattering theories using the MoM. Almost all of this work has been done for one-dimensional (1-D) randomly rough surfaces. Although calculation results using the MoM of the scattering distribution by two-dimensional (2-D) randomly rough surfaces have been reported, it is still a very computationally intense and challenging task.^{23–25} Thus, a well developed and stabilized 1-D analysis is used to determine the domain of validity for approximate scattering methods in this paper.

We will restrict our attention to perfectly conducting surfaces whose surface power spectral density (PSD) function is a Gaussian or exhibits an inverse power law (fractal) behavior. For a surface with a Gaussian PSD function, the random surfaces can be completely characterized by the root-mean-square (rms) surface roughness and the surface auto-covariance (ACV) length. Meanwhile, a fractal surface, having an inverse power law PSD function, can be characterized by three surface parameters.

In Sec. 2, merit functions are introduced for qualitative comparison. In Sec. 3, the numerical comparisons of those approximate methods and the rigorous MoM for Gaussian statistics are shown. In Sec. 4, similar comparisons are

performed for fractal-like surfaces. In Sec. 5, the parameters used for the simulations are presented.

2 Merit Functions

In this paper, we obtain the valid domains of approximate methods by comparing their scattering predictions to the prediction by the rigorous MoM. Thus, it is beneficial to introduce a merit function which enables us to compare quantitatively how close the two predictions are to each other. As an indicator, let us define a linear error given by

$$\varepsilon \equiv \frac{1}{\pi} \frac{\sum_{m=1}^N |I(\theta_m) \Delta\theta_m - I_{\text{MoM}}(\theta_m) \Delta\theta_m|}{\sum_{m=1}^N I_{\text{MoM}}(\theta_m) \Delta\theta_m}, \quad (1)$$

where θ_m is a discretized scattering angle, N is the total number of discretized scattering angles, and I stands for the predicted scattering intensity. Equation (1) is used to calculate the mean error in the predicted scattered radiant power from -90 to 90 deg, normalized by the total scattered radiant power. If the two scattering intensity predictions are exactly the same, the value of the error is zero. On the other hand, it can be some relatively large number if the shapes of the two curves are quite different.

In some applications, the scattering intensity plotted in a logarithmic scale is of interest. With the definition of the error value given in Eq. (1), it is hard to compare quantitatively how the two curves are behaving in the logarithmic scale. Thus, we introduce another merit function which is referred to as the log error given by

$$\varepsilon^* = \frac{1}{N} \sum_{m=1}^N |\log I(\theta_m) - \log I_{\text{MoM}}(\theta_m)|, \quad (2)$$

which gives the mean error of the predicted scattering intensity in the logarithmic scale. In the following sections, the regions of validity of the SPM, KA, and GHS are visualized with the 2-D error maps using these merit functions.

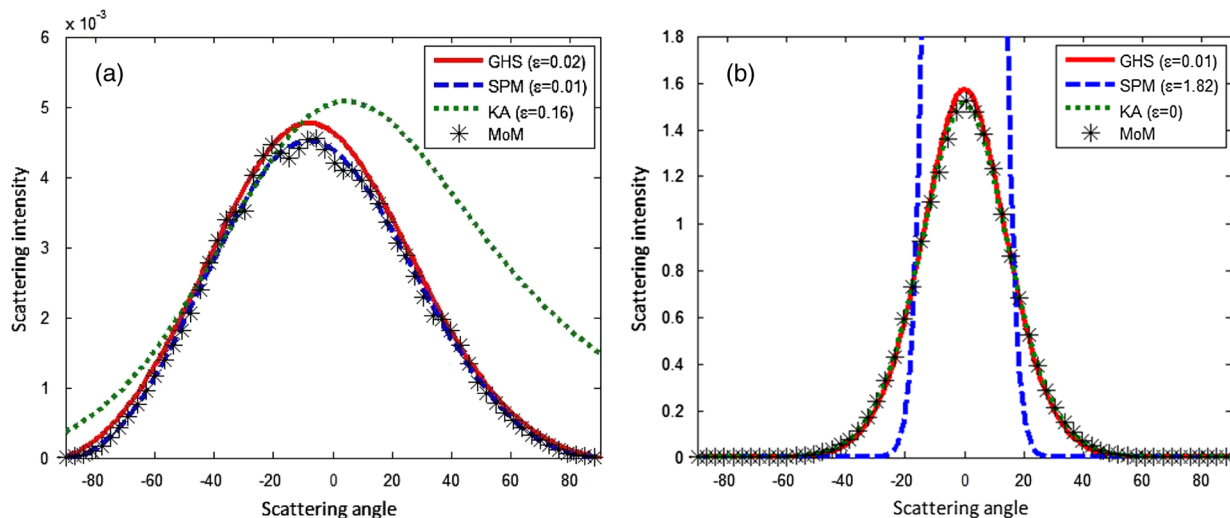


Fig. 1 Scattered intensity of the SPM (dashed line), KA (dotted line), GHS (solid line), and MoM (asterisk) for (a) $\hat{\sigma}_{\text{tot}} = 0.001$, $\hat{l}_c = 0.2$, and $\theta_i = 30$ deg, (b) $\hat{\sigma}_{\text{tot}} = 0.2$, $\hat{l}_c = 2$, and $\theta_i = 0$ deg.

3 Surfaces with a Gaussian Statistics

In this section, the predictions (for TE polarization) of the three approximate methods are compared to the rigorous MoM prediction for 1-D ideally conducting random rough surfaces having Gaussian PSD functions. The wavelength-scaled 1-D Gaussian ACV function is given by

$$\text{ACV}(\hat{x}) = \hat{\sigma}_{\text{tot}}^2 \exp[-(\hat{x}/\hat{l}_c)^2], \quad (3)$$

where \hat{x} is the wavelength-scaled space position, \hat{l}_c is the wavelength-scaled correlation length, and $\hat{\sigma}_{\text{tot}}$ is the wavelength-scaled rms roughness of a random surface. The corresponding 1-D surface PSD function is given by

$$\text{PSD}(\alpha) = \sqrt{\pi} \hat{l}_c \hat{\sigma}_{\text{tot}}^2 \exp[-(\pi \hat{l}_c \alpha)^2], \quad (4)$$

where $\alpha = \sin \theta$ is the x -component of the direction cosine. Since the space position is scaled by the wavelength, its reciprocal variable, the direction cosine, is used for describing surface PSD function instead of the spatial frequency and their relation is given by $f_x = \alpha/\lambda$, where f_x is the x -component of the spatial frequency and λ is the wavelength of the incident light.

For a surface with a Gaussian surface PSD, the rms roughness, the surface ACV length, and the incident angle are the three parameters affecting scattered light behavior. Our numerical analysis is limited to the practical range of surface parameters defined by $0 < \hat{\sigma}_{\text{tot}} < 1$ and $0 < \hat{l}_c < 3$. The accuracy of the MoM results in this region is discussed in Sec. 5.

3.1 Scattering Intensity Distribution

Figure 1 shows the incoherent scattered intensity distribution predicted by the SPM (blue-dashed line), KA (green-dotted line), GHS (red solid line), and MoM (black asterisk) for two different sets of surface parameters. In Fig. 1(a), the case of $\hat{\sigma}_{\text{tot}} = 0.01$, $\hat{l}_c = 0.2$, and $\theta_i = 30$ deg, which is a smooth surface with a short-correlation length, is considered. The predictions of both the SPM and GHS agree well with the MoM prediction, and the KA result agrees near the specular direction but fails in the wide-angle regime. In particular, it

does not converge to zero at ± 90 deg scattering angles, which is a nonphysical situation. The case of $\hat{\sigma}_{\text{tot}} = 0.2$, $\hat{l}_c = 2$, and $\theta_i = 0$ deg, which is moderately rough with a long-correlation length, is illustrated in Fig. 1(b), and both the intensity profiles from KA and GHS methods show a good agreement to the MoM prediction; however, as expected, the SPM fails for this moderately rough surface.

Figures 2(a) and 2(b) illustrate two different situations where the GHS model has reasonable accuracy for moderately rough surfaces, but the other two fail to predict an accurate intensity distribution. However, they fail for different reasons; the SPM fails because the smooth-surface approximation is violated and the KA fails because the small correlation lengths produce large angle scattering that violates the paraxial limitation. Figures 2(c) and 2(d) show for even rougher surfaces and thus, the SPM predictions have been omitted. Figure 2(c) shows the predicted intensity distribution by the KA and GHS for the case of $\hat{\sigma}_{\text{tot}} = 0.4$, $\hat{l}_c = 2.5$, and $\theta_i = 50$ deg. The GHS predictions agree well with the rigorous MoM predictions over the entire range of scattered angles; however, the KA prediction exhibits a significant error near the peak and in the forwarding scattering direction due to the large (nonparaxial) incident angle. In Fig. 2(d), a very rough surface ($\hat{\sigma}_{\text{tot}} = 1$) is considered, and the overall angular behavior predicted by the GHS theory is quite close

to that predicted by the rigorous MoM except near the specular direction where the MoM predictions exhibit irregularities due to the considerable multiple scattering.²⁶ There is no specular beam for such a rough surface, i.e., the total integrated scatter is approximately unity. The KA method fails badly due to the large surface roughness. Extensive empirical scatter predictions with the KA method have indicated that it remains quite accurate, at this correlation width, for $\hat{\sigma}_{\text{tot}} \leq 0.5$. This statement will be validated later in Fig. 3(b).

3.2 Comparative Visualization of the Domain of Validity

To quantitatively illustrate the relative accuracy of the three approximate surface scatter models, we calculate the linear-error values and illustrate the value as a corresponding gray level in a 2-D surface parameter space. Figure 3 illustrates contour maps of this linear error over the surface parameter space for each of the approximate theories with the normal incidence. Note that, for our simulation of scattered intensity with the MoM, one thousand realizations were used and the averaged intensity of the MoM predictions still exhibits minor fluctuations.

The SPM has a high accuracy over the entire range of correlation widths; however, the domain is severely restricted

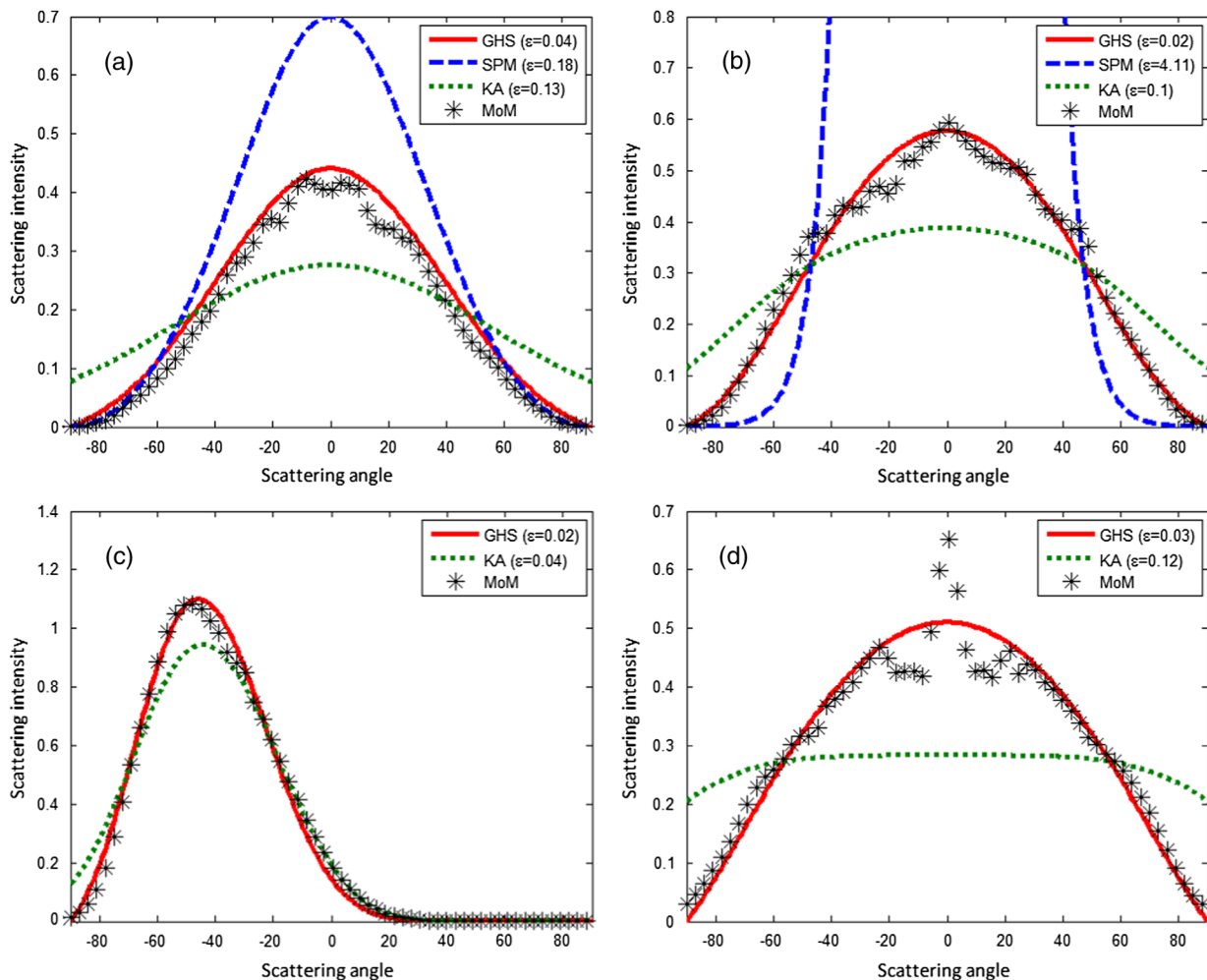


Fig. 2 Scattered intensity for (a) $\hat{\sigma}_{\text{tot}} = 0.1$, $\hat{l}_c = 0.25$, and $\theta_i = 0$ deg, (b) $\hat{\sigma}_{\text{tot}} = 0.3$, $\hat{l}_c = 0.8$, and $\theta_i = 0$ deg, (c) $\hat{\sigma}_{\text{tot}} = 0.4$, $\hat{l}_c = 2.5$, and $\theta_i = 50$ deg (d) $\hat{\sigma}_{\text{tot}} = 1$, $\hat{l}_c = 2$, and $\theta_i = 0$ deg. The SPM prediction is not plotted in (c) and (d).

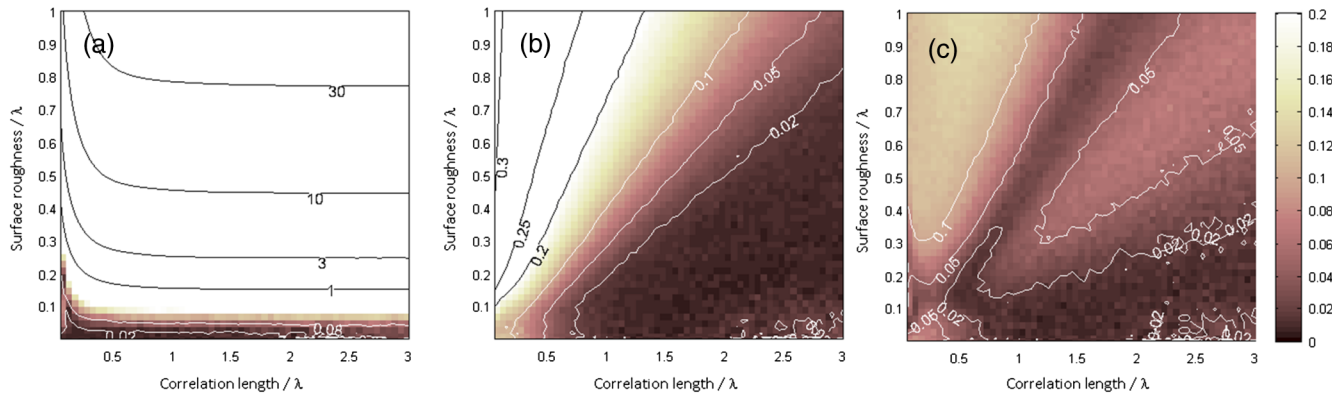


Fig. 3 Error contour maps at normal incidence: (a) the SPM, (b) KA, and (c) GHS.

to very smooth surfaces as shown in Fig. 3(a). The KA can be considered to have a high degree of accuracy over a much larger fraction of the 2-D surface parameter space, increasing almost linearly to moderately rough surfaces for an increasing correlation length as shown in Fig. 3(b). However, the KA prediction is quite inaccurate ($\varepsilon > 0.2$) over a significant fraction of the domain represented by the upper left corner of Fig. 3(b). Meanwhile, the GHS theory exhibits slightly less accuracy than the SPM and KA in some regions of their domain of validity, but it has a much broader valid domain in general. For example, the entire illustrated domain is valid if $\varepsilon < 0.2$ is considered as the criterion as illustrated in Fig. 3(c).

It is widely believed that the validity of the KA method depends on the curvature of the surface irregularities making up the surface profile.^{6,10,26} Due to the tangential plane approximation, the KA is considered to be accurate when the curvature is less than the wavelength of interest. In Fig. 4(a), the numerically calculated contour lines of the rms slope of the surface are plotted on the top of the error map previously shown in Fig. 3(b). In Fig. 4(b), contour lines of the rms curvature are plotted on the top of the same error map. From the two figures, it is clear that the validity of the KA method is more strongly correlated to the rms slope than to the rms curvature of the surface.

Likewise, in Fig. 5(a), the numerically calculated contour lines of the rms slope of the random surface are plotted on the top of the error profile map shown in Fig. 3(c). For normally incident light, the GHS method is relatively accurate when the rms slope of the randomly rough surfaces is less than unity. Figure 5(b) indicates that for a 40-deg incident angle, the value of the error increases for a given value of the rms slope. This degradation in accuracy with an increasing incident angle may be caused by the fact that the GHS theory does not consider shadowing effects and multiple scattering.

In order to more clearly show the incident angle dependency of the region of validity for the three approximate theories, error maps similar to those shown in Fig. 3 at normal incidence are provided in Fig. 6 for the incident angles of 20, 40, and 60 deg. The shifting of the error contour lines with an increasing incident angle can be studied; however, if an error value of $\varepsilon < 0.2$ is maintained as a criterion for validity, the entire domain of 2-D surface parameter space illustrated remains valid for the GHS theory at $\theta_i = 20$ deg and at $\theta_i = 40$ deg. Not until $\theta_i = 60$ deg does a portion of this domain (upper central) exhibit an error value greater than $\varepsilon = 0.2$. However, within the small slope regime (lower right), it still shows a small error value, $\varepsilon < 0.05$, for very large incident angles. It can be seen in Fig. 6 that, if a

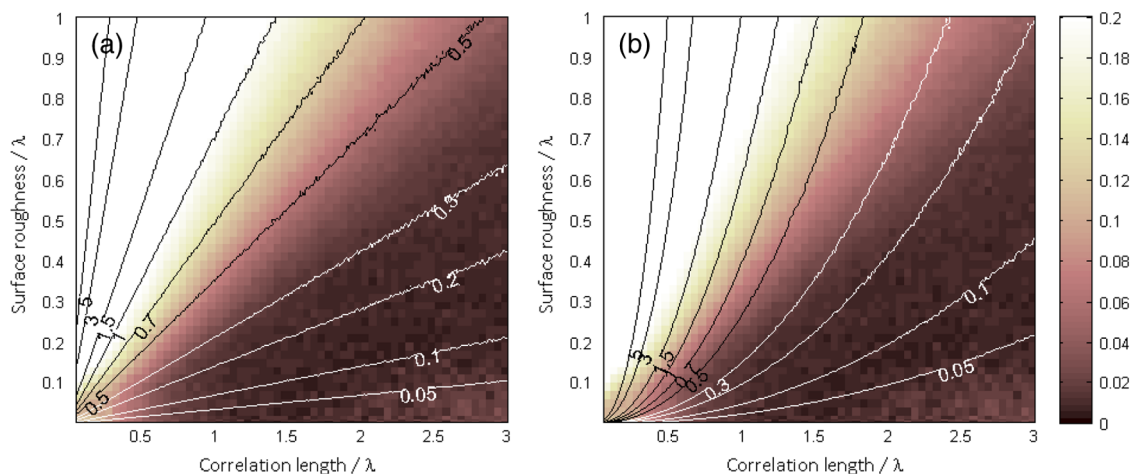


Fig. 4 Contour lines of (a) the rms slope and (b) rms curvature of random surfaces superposed on the top of the error map for the KA method with the normally incident light.

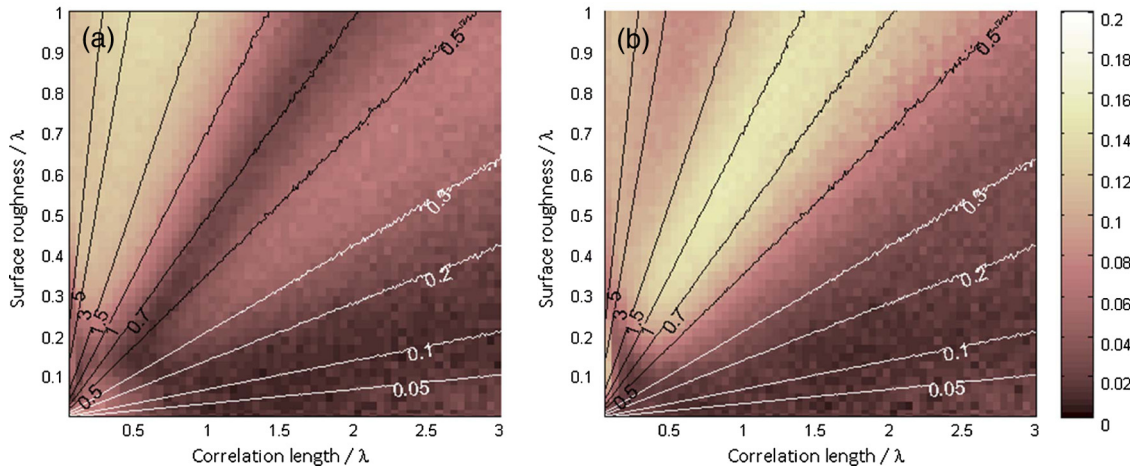


Fig. 5 Contour lines of the rms slope superposed on the top of the error map of the GHS theory for (a) $\theta_i = 0$ deg and (b) $\theta_i = 40$ deg.

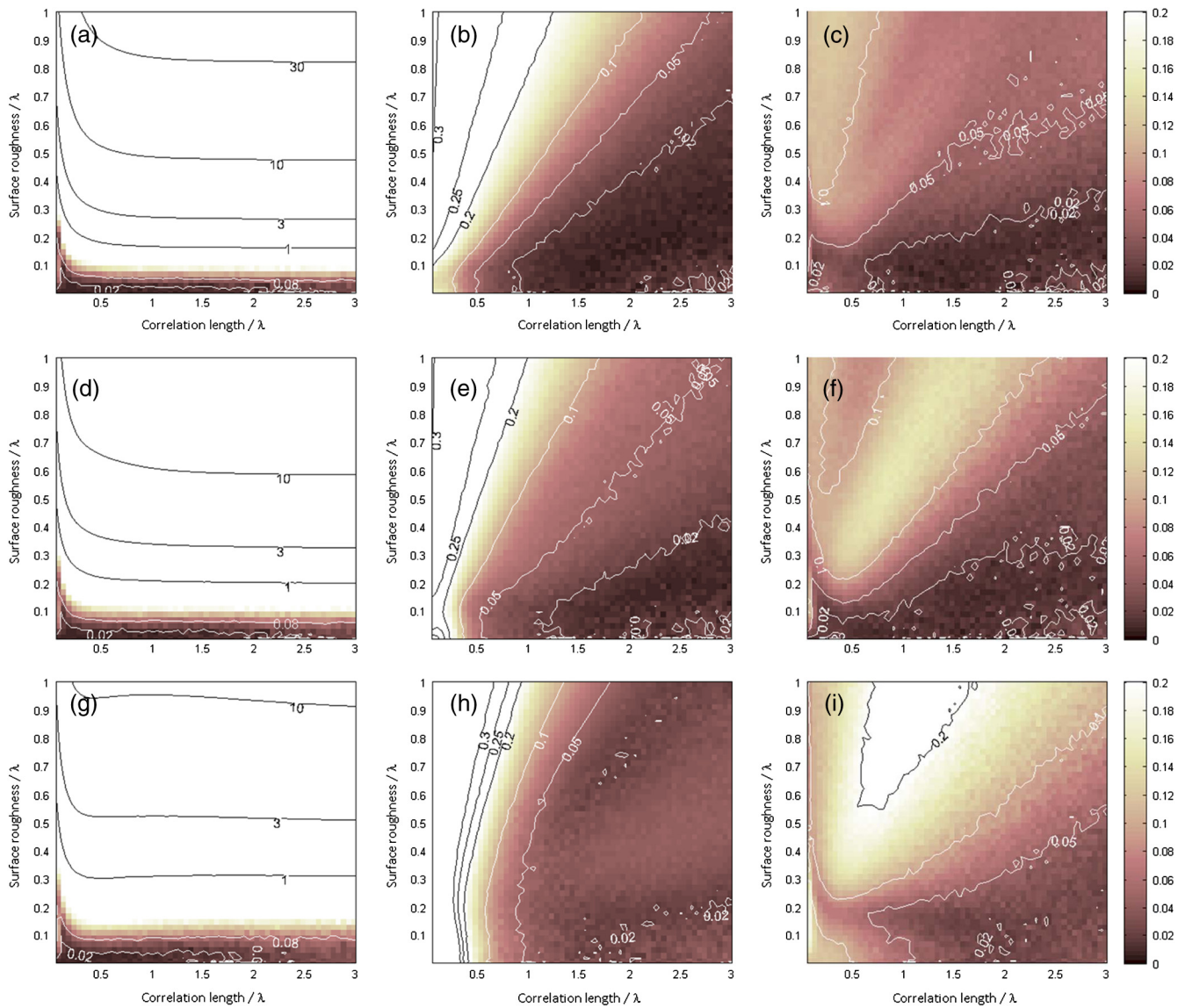


Fig. 6 Error contour maps for the SPM with (a) $\theta_i = 20$ deg, (d) $\theta_i = 40$ deg, and (g) $\theta_i = 60$ deg, for the KA with (b) $\theta_i = 20$ deg, (e) $\theta_i = 40$ deg, and (h) $\theta_i = 60$ deg, and for the GHS with (c) $\theta_i = 20$ deg, (f) $\theta_i = 40$ deg, and (i) $\theta_i = 60$ deg.

different criterion for validity is chosen, or if a particular region in the domain is of interest, the KA theory may actually be more accurate than the GHS theory.

In this section, scattering intensity predictions by the SPM, KA, and GHS are compared to the rigorous MoM predictions for surfaces having Gaussian surface PSD for the 1-D TE polarization case. Using the linear-error value, the region of validity of those three approximate theories is obtained in surface parameter space. The domain of validity of the SPM is largely restricted to the smooth surface criterion, but the domain is broadened as the angle of incidence is increased. The domain of the KA depends on the rms slope of the random surfaces and it shrinks as the angle of incidence is increased. Regarding the GHS method, its domain of validity is broader than the other two approximate methods and it becomes smaller when the incident angle is larger.

4 Surfaces with an Inverse Power Law PSD

The valid domain of the SPM and KA has been studied by many previous researchers. However, most of their studies have focused on surfaces whose PSD function is a 1-D Gaussian function.^{9–14,16–19} But it is known that well-polished optical surfaces have a fractal structure for which the surface PSD function follows an inverse power law^{27–30} behavior.

There are a few researchers who have studied scattering by fractal surfaces^{20,27,31–35} but, unlike previous researchers, we obtain the valid domain by directly comparing the scattering predictions of approximate methods with the rigorous MoM. The valid domain is represented in terms of the parameters which characterize the fractal surfaces.

The surface PSD of a fractal surface may follow the inverse power law given by

$$\text{PSD}(\alpha) = C_0 |\alpha|^{-c}, \quad (5)$$

where C_0 is some constant and c is the slope of the surface PSD function in log–log scale. Again, the surface PSD function is represented in terms of the direction cosine instead of the spatial frequency. Typically, surfaces have a finite size, thus its surface PSD function has a low frequency limit. Moreover, when generating a surface profile numerically, there must be a high frequency limit. With those reasons, the Weierstrass–Mandelbrot (WM) function^{34,35} is usually used to generate a fractal surface profile. However, in approximate models, predicting the scattered intensity for finite size surfaces requires one to calculate edge effects. These edge effects complicate the simple formula which is the strongest aspect of the SPM, KA, and GHS. In this paper, instead of using the WM function, the abc -function PSD is employed as an approximate surface PSD of fractal surfaces. The 1-D abc -function is given by

$$\text{PSD}(\alpha) = \frac{a}{(1 + b^2 \alpha^2)^{c/2}}, \quad (6)$$

where a and b are constants given by the surface statistical properties. Due to the shape of the function in log–log scale, $1/b\lambda$ is called the shoulder frequency. Since the function converges to a certain value when the frequency approaches zero, the total rms roughness $\hat{\sigma}_{\text{tot}}$ is given by

$$\hat{\sigma}_{\text{tot}} = \sqrt{2} \times \left[\frac{a\sqrt{\pi}}{b(c-1)} \frac{\Gamma((c+1)/2)}{\Gamma(c/2)} \right]^{1/2}, \quad (7)$$

when the slope parameter c is larger than unity. Here, Γ is the gamma function. Its 1-D Fourier transform gives an analytic expression for the ACV function

$$\text{ACV}(\hat{x}) = 2 \times \sqrt{2\pi} \frac{a}{b} \frac{2^{-c/2}}{\Gamma(c/2)} \left(\frac{2\pi|\hat{x}|}{b} \right)^{(c-1)/2} \times K_{(c-1)/2} \left(\frac{2\pi|\hat{x}|}{b} \right), \quad (8)$$

where K is the modified Bessel function of the second kind. Since the function behavior follows the inverse power law where the frequency is larger than the shoulder frequency, the abc -function has been used to model the PSD of fractal surfaces.³⁶ Note that, since we are using the wavelength-scaled space coordinate, the surface parameters a , b , and c are all dimensionless quantities in this paper.

Basically, random surfaces for which the surface PSD is an abc -function can be characterized by the a , b , and c parameters. However, in this paper, the three parameters that are the rms roughness $\hat{\sigma}_{\text{tot}}$, the slope parameter c , and the shoulder “frequency” b are used for characterizing surfaces for comparison purposes and those two parameter sets have a one to one correspondence. In addition, we fixed the b value as 20 because the number of sampling points for numerical calculation is limited. However, the comparison with different shoulder frequencies is shown at the end of this section.

4.1 Scattering Intensity Distribution

Figure 7 shows the incoherent scattered intensity distributions predicted by the SPM (blue dashed), KA (green dotted), GHS (red solid), and MoM (black asterisk) for the case of (a) $\hat{\sigma}_{\text{tot}} = 0.025$, $c = 1.4$, and $\theta_i = 40$ deg and (b) $\hat{\sigma}_{\text{tot}} = 0.6$, $c = 2.8$, and $\theta_i = 0$ deg in the logarithmic scale. In Fig. 7(a), since the rms roughness is small, both the SPM and MoM results agree with each other as expected. The log-error value of the SPM is $\varepsilon^* = 0.03$ which is quite a smaller value than those of the KA ($\varepsilon^* = 0.47$) and GHS ($\varepsilon^* = 0.07$). In Fig. 7(b), the surface is quite rough and the SPM is out of its valid domain, but the KA shows a good agreement near the specular direction. However, the KA prediction fails at the large scattering angles leading to a log-error value $\varepsilon^* = 0.20$. In both cases, the GHS prediction shows a quite good agreement not only near the specular direction and but also over the whole range of scattering angles.

Figure 8 shows the predicted scattered intensity for three different cases of surface parameter sets. In Fig. 8(a), the scattering intensity distributions for the case of $\hat{\sigma}_{\text{tot}} = 0.1$, $c = 1.4$, and $\theta_i = 40$ deg are plotted in the logarithmic scale and the SPM shows a good agreement to the MoM except near specular direction leading to $\varepsilon^* = 0.07$. It is quite interesting that the SPM prediction agrees well at the large scattering angles even when the rms roughness is not quite small. Regarding the GHS, its prediction is superior near the specular direction than the prediction by the SPM, but it predicts little stronger scattering at large scattering angles leading to $\varepsilon^* = 0.09$. If the distribution is plotted

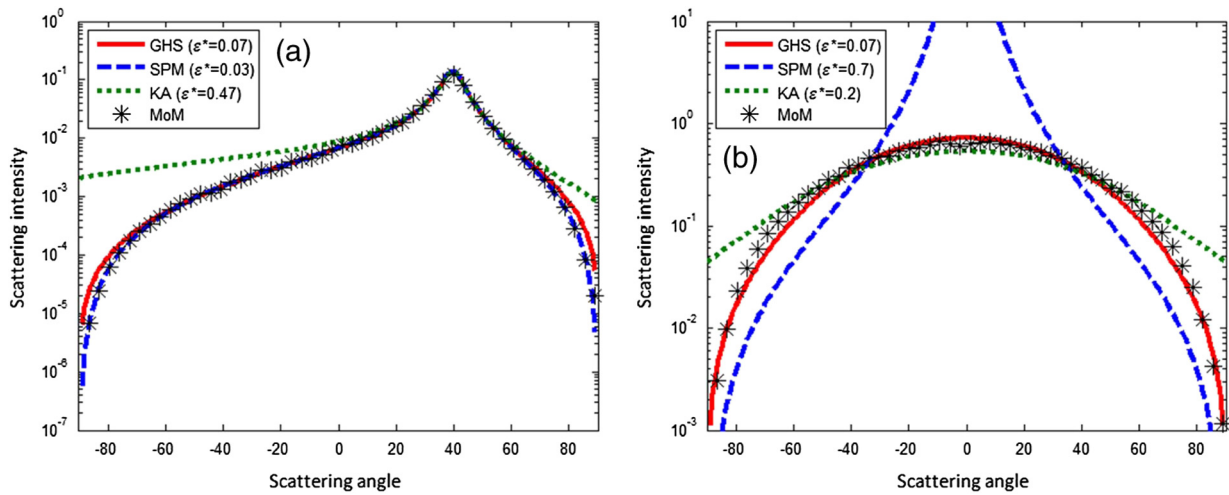


Fig. 7 Scattering intensity distributions by the SPM, KA, GHS, and MoM for the case of (a) $\hat{\sigma}_{tot} = 0.025$, $c = 1.4$, and $\theta_i = 40$ deg and (b) $\hat{\sigma}_{tot} = 0.6$, $c = 2.8$, and $\theta_i = 0$ deg in the logarithmic scale.

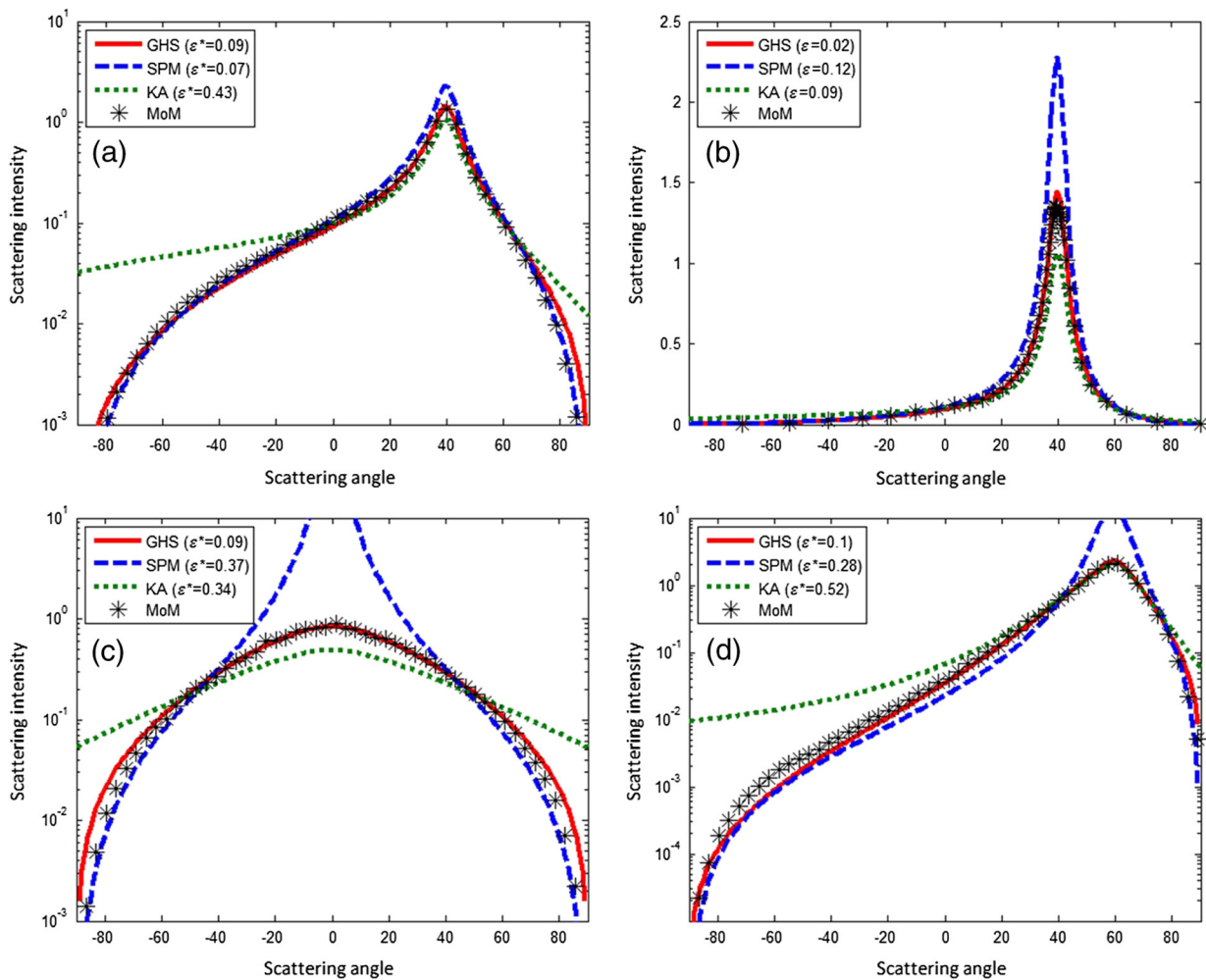


Fig. 8 Scattering intensity distributions by the SPM, KA, GHS, and MoM for the case of (a) $\hat{\sigma}_{tot} = 0.1$, $c = 1.4$, and $\theta_i = 40$ deg in the logarithmic scale, (b) the surface parameters are the same to those of (a) but scattering intensity is plotted in linear scale, (c) $\hat{\sigma}_{tot} = 0.3$, $c = 2$, and $\theta_i = 0$ deg in the logarithmic scale (d) $\hat{\sigma}_{tot} = 0.3$, $c = 2.8$, and $\theta_i = 60$ deg in the logarithmic scale.

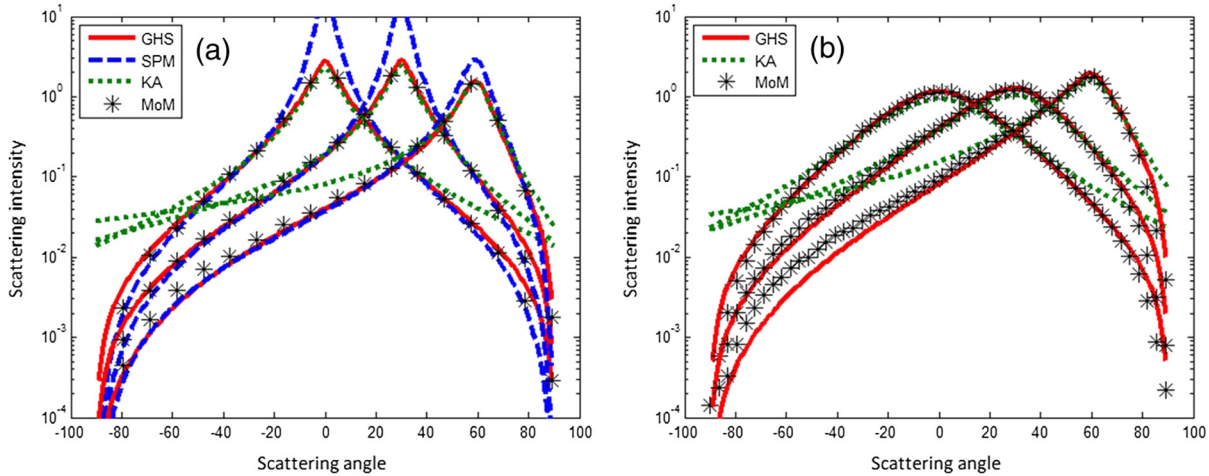


Fig. 9 Scattering intensity distributions by the SPM, KA, GHS, and MoM for the case of (a) $\hat{\sigma}_{\text{tot}} = 0.15$, $c = 2$, and $\theta_i = 0$ deg and (b) $\hat{\sigma}_{\text{tot}} = 0.3$, $c = 2.4$, and $\theta_i = 0$ deg.

in linear scale as in Fig. 8(b), it is obvious that the SPM overestimates the scattering near the specular direction, but the GHS and KA predict quite accurate values at that direction. This results in a linear-error value of the SPM, KA, and GHS of $\varepsilon_{\text{SPM}} = 0.12$, $\varepsilon_{\text{KA}} = 0.09$, and $\varepsilon_{\text{GHS}} = 0.02$, respectively. Figure 8(c) shows the scattering predictions for the case of $\hat{\sigma}_{\text{tot}} = 0.3$, $c = 2$, and $\theta_i = 0$ deg, whose rms roughness is moderately large. The SPM fails to predict the scattered intensity properly near specular direction and the KA fails to accurately predict the scattered intensity both near specular direction and at large scattering angles. In Fig. 8(d), the rms roughness is the same as Fig. 8(c) but the slope is larger ($c = 2.8$). Again, the SPM overestimates scattering near the specular direction, and the KA prediction deviates at the large scattering angles. However, in both the cases of Figs. 8(c) and 8(d), the GHS has good accuracy over all scattering angles for both small and relatively large incident angle cases.

Figure 9 shows the dependency of the validity of the SPM, KA, and GHS with the variations in incident angle for the two surface parameter sets. In Fig. 9(a), the scattered intensity distributions for the 0, 30, and 60 deg of incident angle for the case of $\hat{\sigma}_{\text{tot}} = 0.15$ and $c = 2$ are provided. The SPM predicts overly stronger scattering at the specular direction and the amount of incorrectness is reduced when the angle of incidence becomes larger. The KA prediction shows a good agreement to the rigorous MoM result near the specular direction but its large scattering angle behavior is very inaccurate regardless of incident angle. The GHS predictions agree quite well with the rigorous MoM result over all scattering angles and for all the three incident angles; however, the predictions are slightly high at large scattering angles. Figure 9(b) illustrates the scattering predictions for the surface whose roughness and the slope parameter c values are larger than the previous one ($\hat{\sigma}_{\text{tot}} = 0.3$ and $c = 2.4$) and the overall shape of the scattering distribution is less sharply peaked in the specular direction than the case of Fig. 9(a). Similarly to Fig. 9(a), the KA prediction is valid only near the scattering angle, but the GHS predicts quite accurately not only at the specular ray direction but also at large scattering angles. Note that in Fig. 9(b), the SPM results are not plotted.

4.2 Comparative Visualization of the Domain of Validity

To reveal the dependency of the validity of the SPM according to the surface parameters, both the log- and linear-error values for the SPM with the normal incidence are calculated and shown in Figs. 10(a) and 10(b), respectively. Figure 10(b) shows that the validity of the SPM is largely restricted to smooth surface criteria regardless of the slope parameter. However, if the log-error values are calculated as shown in Fig. 10(a), the valid region of the SPM is dramatically broadened. This can be explained by the fact that, as shown in the previous section, the scattering intensity distribution at large angles predicted by the SPM agrees very well to the rigorous MoM prediction not only for the surface whose rms roughness is very small but also moderately large.

Figure 11 shows error maps for the KA using (a) the log-error values and (b) the linear-error values at normal incidence. In Fig. 11(b), the KA prediction can be considered to be valid where the ratio of the rms roughness to the slope parameter is small. However, when the log-error value is calculated, Fig. 11(a) indicates that the KA fails to make accurate predictions over almost the entire surface parameter domain. This characteristic results from the fact that the KA prediction shows relatively good agreement to the prediction of the MoM near the specular direction when the ratio of the rms roughness to the slope parameter is small, but it overestimates the large angle scattering over almost the entire surface parameter domain.

The log- and linear-error values for the GHS theory are calculated and illustrated in Fig. 12. In Fig. 12(b), similar to Fig. 11(b), the calculated error values are smaller when the ratio of the rms roughness to the slope parameter is smaller. However, the valid domain of the GHS is much broader than that of the KA. In Fig. 12(a), comparing to Fig. 10(a), the log-error values for the GHS are larger than those for the SPM in some regions and it comes from the fact that the GHS overestimates the large angle scattering. However, the error map in Fig. 12(a) shows that the prediction of the GHS show a good agreement to the rigorous MoM prediction in linear scale over the larger surface parameter domain than the other two approximate methods with reasonable accuracy.

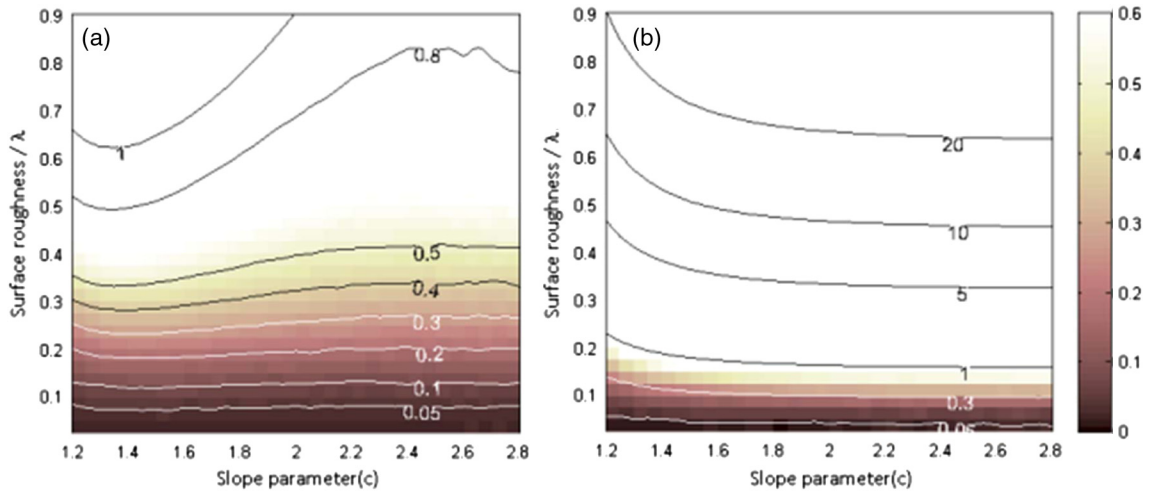


Fig. 10 (a) SPM log-error map and (b) SPM linear-error map for the normal incidence.

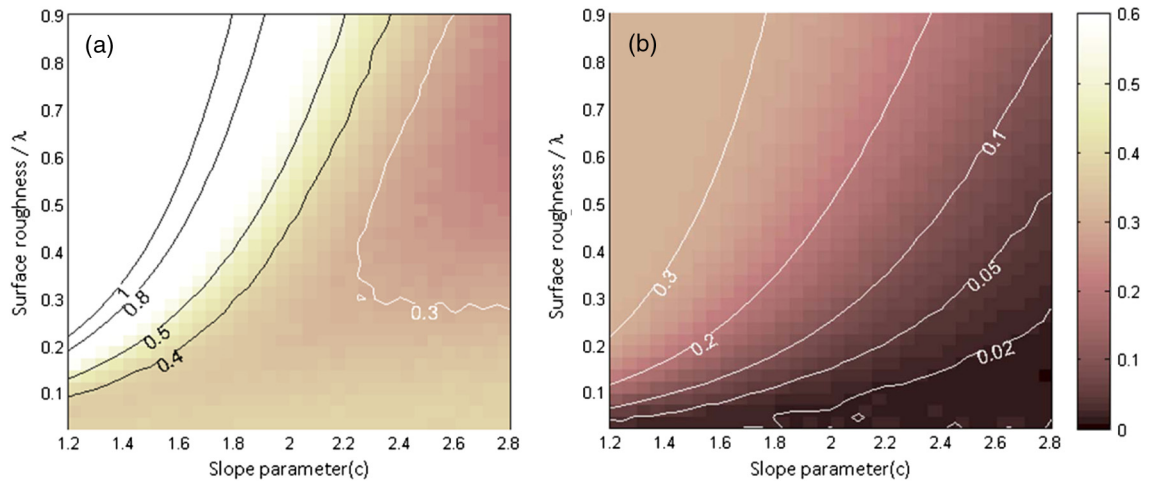


Fig. 11 (a) KA log-error map and (b) KA linear-error map for the normal incidence.

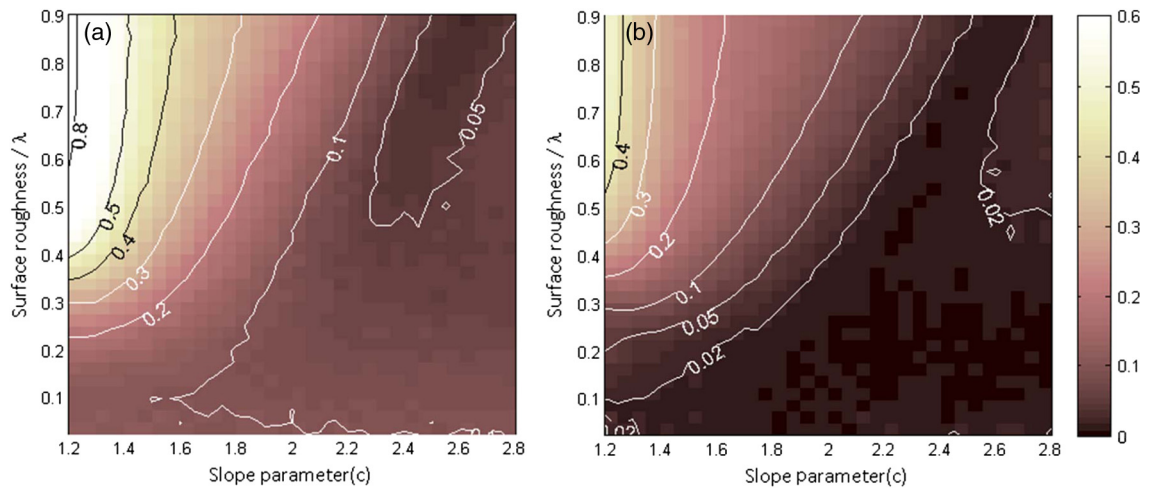


Fig. 12 (a) GHS log-error map and (b) GHS linear-error map for the normal incidence.

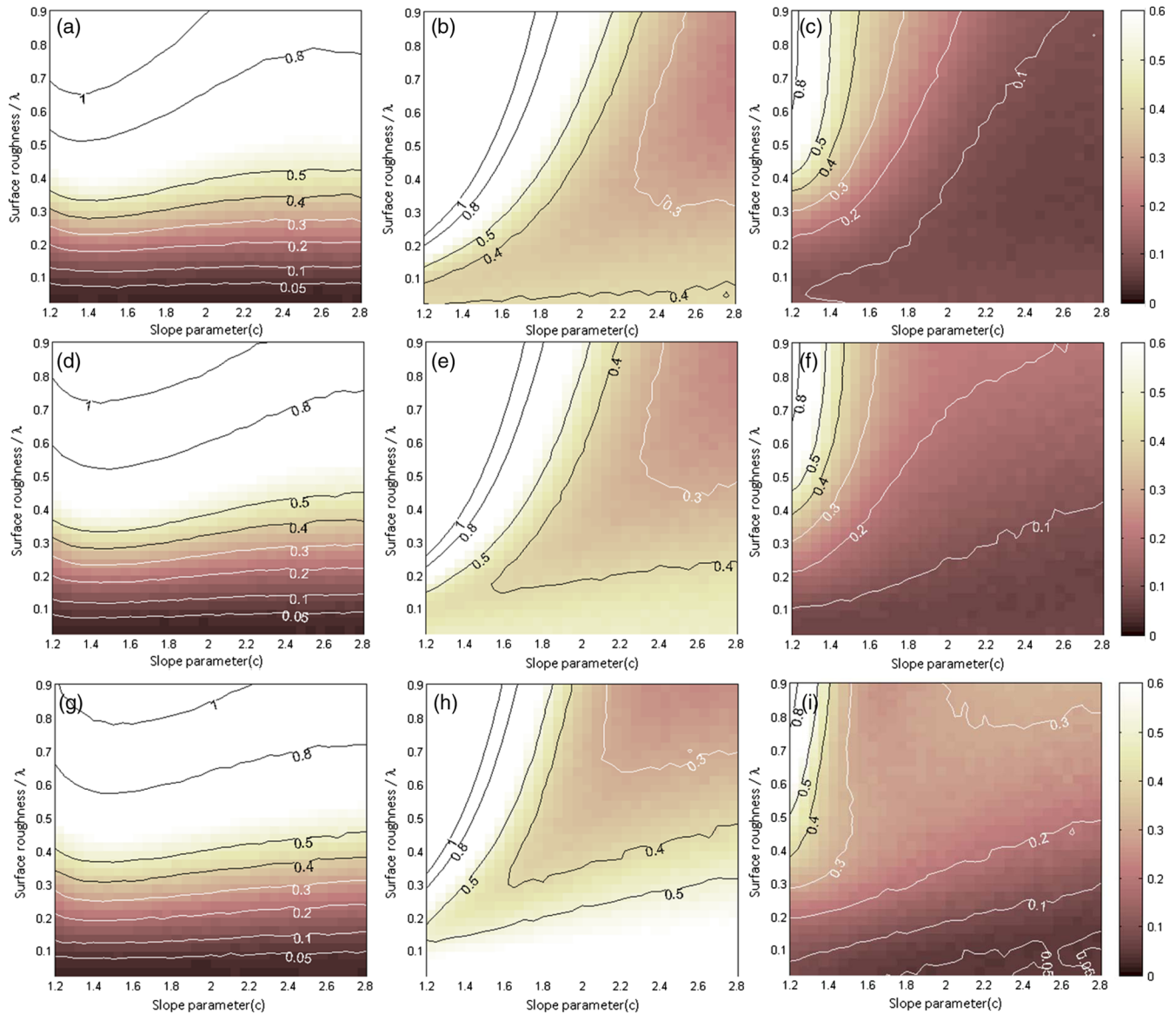


Fig. 13 SPM log error map (a) $\theta_i = 20$ deg, (d) $\theta_i = 40$ deg, and (g) $\theta_i = 60$ deg; KA log error map (b) $\theta_i = 20$ deg, (e) $\theta_i = 40$ deg, and (h) $\theta_i = 60$ deg; and GHS log error map (c) $\theta_i = 20$ deg, (f) $\theta_i = 40$ deg, and (i) $\theta_i = 60$ deg.

In order to compare the incident angle dependency of the region of validity for the SPM, KA, and GHS, the error maps using log-error values for the three methods in the case of $\theta_i = 20, 40,$ and 60 deg are shown in Fig. 13. The valid domain of the SPM appears that it is not significantly affected by the change of the incident angle. Meanwhile, for both the GHS and KA, the valid area in the domain reduces with an increasing incident angle. But, in these three incident angle cases, the error maps show that the GHS theory again has a wider range of validity for large incident angles than those of the KA method.

4.3 Scattering Intensity Distribution for Different Shoulder Frequencies

In the previous sections, the value of the parameter b is fixed to 20. In this section, the scattered intensity comparison is performed for different b parameter values. Figure 14(a) shows the surface PSD function of the three surfaces. The

surface A has 0.02λ of rms roughness with $b = 20$, the surface B has 0.045λ of rms roughness with $b = 100$, and the surface C has 0.14λ of rms roughness with $b = 500$. All the three surfaces have the same slope parameter c value of 2. Figure 14(b) shows the rigorous MoM predictions in log-log scale at normal incidence and it shows that different shoulder frequencies with the same slope parameter change only the small angle scattering behavior.

Figure 15(a) shows the predicted scattering distribution for the surface A in the case of $\theta_i = 0$ deg and $\theta_i = 60$ deg for the four different methods. Since the rms roughness is small, the SPM predicts quite accurate results, the GHS has reasonable accuracy for entire scattering and incident angles, and the KA has a good agreement near specular direction, but fails to predict at large angle scattering behavior. This trend holds for the surface B as shown in Fig. 15(b) where the rms roughness is moderately larger and the b parameter value is also moderately smaller than the case of Fig. 15(a).

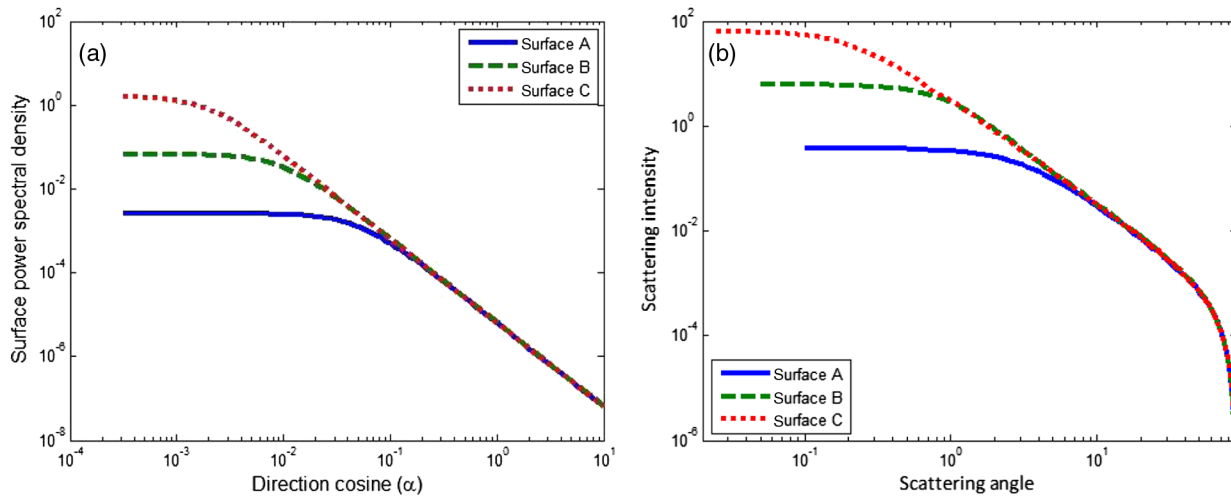


Fig. 14 (a) Surface PSD functions for the surface A, B, and C with the same slope parameter $c = 2$ and different b parameter values. (b) The scattering intensity distributions predicted by the MoM for the three surfaces in log–log scale at normal incidence.

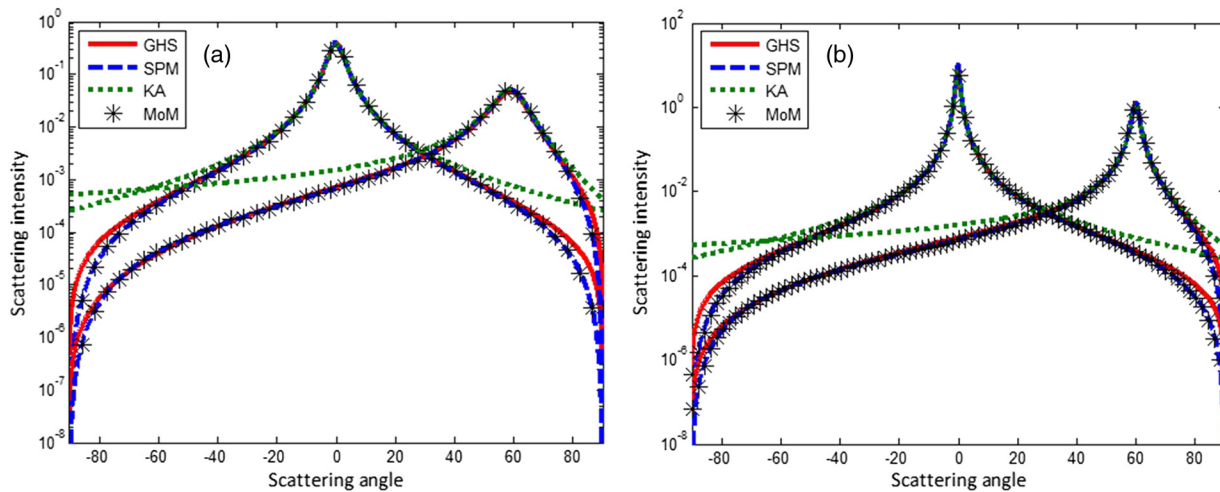


Fig. 15 Predicted scattering intensity distributions by the SPM, KA, GHS, and MoM in the case of $\theta_i = 0$ deg and $\theta_i = 60$ deg for (a) the surface A and (b) the surface B.

Figure 16(a) shows the predicted scattered intensity for the surface C whose shoulder frequency is much smaller and rms roughness is much larger than surfaces A and B. The behavior of the scattered intensity is very strongly peaked in the specular direction when plotted in a linear-log scale. That the SPM fails to accurately predict the scattered intensity near the specular direction is shown in the log–log plot of Fig. 16(b). The GHS and KA theories show a good agreement with the rigorous MoM prediction as shown in Fig. 16(b). But unlike the KA, the GHS predicts reasonably accurate predictions at large scattering angles as well as near specular direction as shown in Fig. 16(a).

Due to the limitation of the computer memory and computation time, the simulation for the surface with much smaller shoulder frequency is not calculated. However, as shown in this section, it is strongly possible that the trend of the region of validity obtained with $b = 20$ still holds for the cases with much smaller shoulder frequency. The full analysis of the region of validity for different shoulder frequencies remains a topic for later research.

5 Simulation Parameters

Throughout the previous two sections, the predictions by the three approximate theories were compared to the predictions by the rigorous MoM. The formalism of the MoM is well known, but the parameters used for the calculations must be presented. Regarding the simulation for surfaces with a Gaussian surface PSD, to show the behavior of the error values in the domain of interest, 55 cases were selected for rms roughnesses from 0.002λ to 1λ . For every roughness case, 60 cases of the correlation length from 0.05λ to 3λ were calculated. The total length of the surface was chosen to be 20λ and 1000 realizations were carried out. A tapered incident wave was used and the tapering parameters were chosen to be one-fourth of the surface length.³⁴ The total number of sampling points was carefully chosen depending on the correlation length and roughness. In our experience, the total number of sampling points which is required to achieve energy conservation depends more on the rms slope of the random surface than its correlation length. Sixteen sampling points per wavelength were used for surfaces having rms

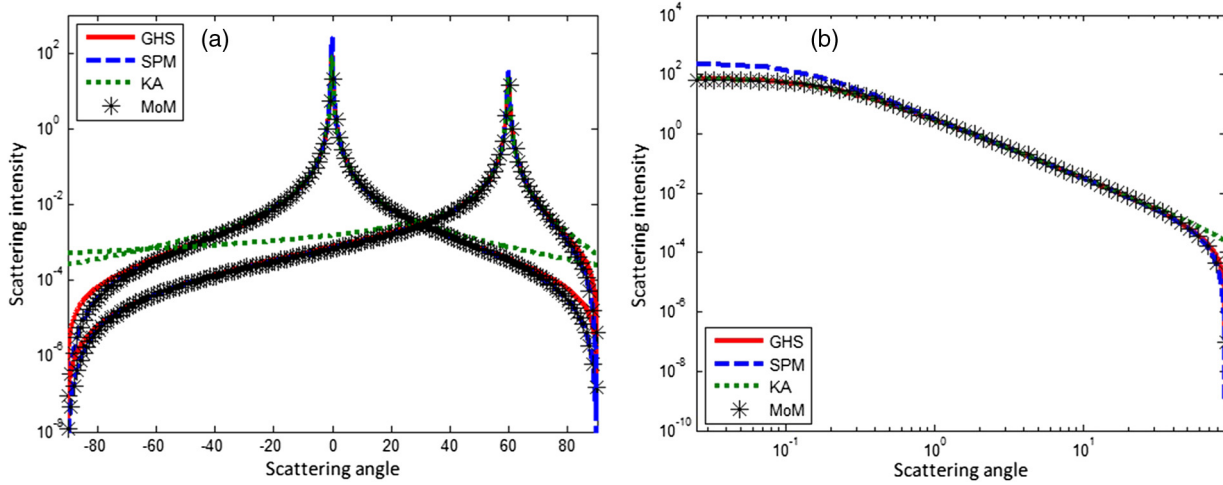


Fig. 16 Predicted scattering intensity distributions by the SPM, KA, GHS, and MoM for surface C in the case of (a) $\theta_i = 0$ deg and $\theta_i = 60$ deg in linear-log scale and (b) $\theta_i = 0$ deg in log–log scale.

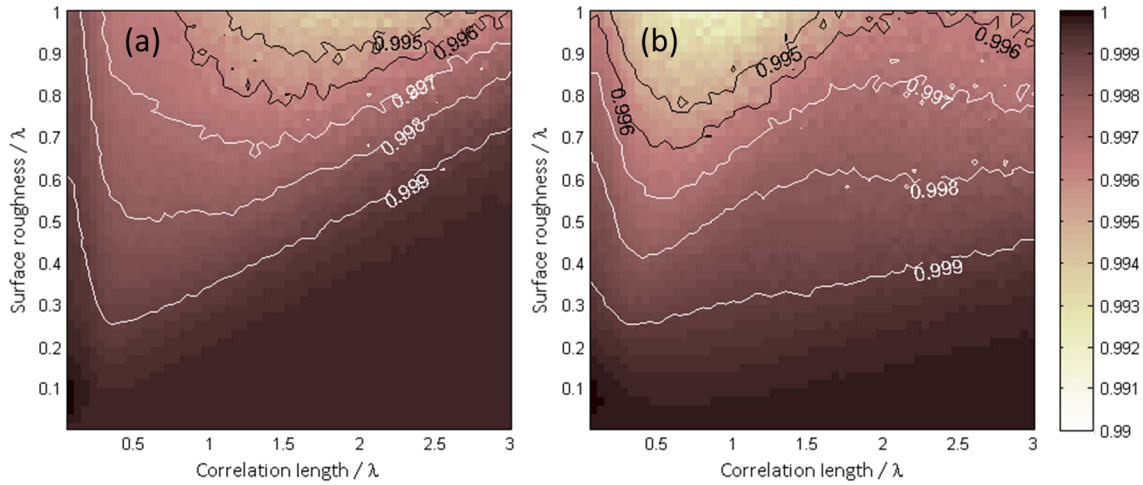


Fig. 17 Contour map of total fractional reflected energy as a function of rms roughness and surface correlation length for the MoM: (a) $\theta_i = 0$ deg and (b) $\theta_i = 40$ deg.

slopes smaller than unity, and a denser sampling ratio is used for the case of steeper rms slopes. However, due to the restriction of the memory and running time, no >2000 total sampling points were used. Thus, in the regime of short-correlation length and very steep mean slope, the reliability of the MoM results is possibly reduced. Figure 17(a) shows the total fractional reflected energy predicted by the MoM for the normal incidence case and Fig. 17(b) is for a 40-deg incident angle case. In both figures, the energy conservation condition is achieved with $<0.5\%$ error over almost the entire surface parameter domain of interest. However, it must be mentioned that, although energy conservation is one of the necessary conditions, the fulfillment of the requirement does not always guarantee the accuracy of the method.

Regarding the simulation parameters for surfaces with an *abc*-function surface PSD, both the number of the sampling points per wavelength ($\lambda/\Delta x$) and the surface length is carefully selected. The former is related to the highest frequency limit and the latter is related to the lowest frequency limit of the surface PSD. When it comes to surface length, the surface length is chosen to be 40λ to 60λ in order that the lowest

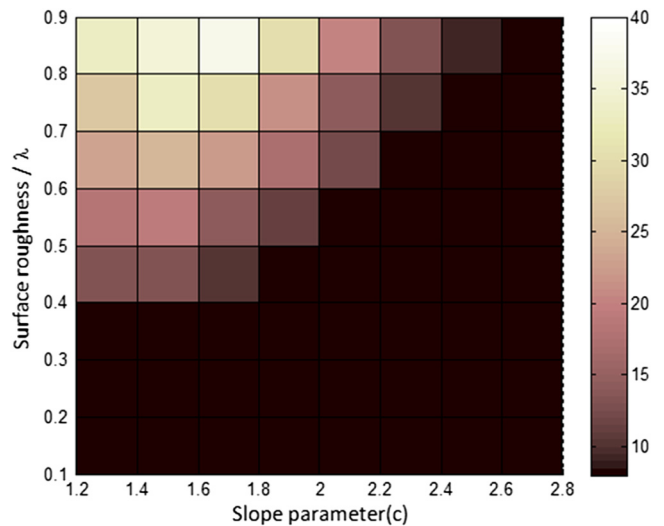


Fig. 18 Selected minimum number of the sampling points per wavelength for the 9×9 cases of the surface parameter sets (c, σ_{tot}) .

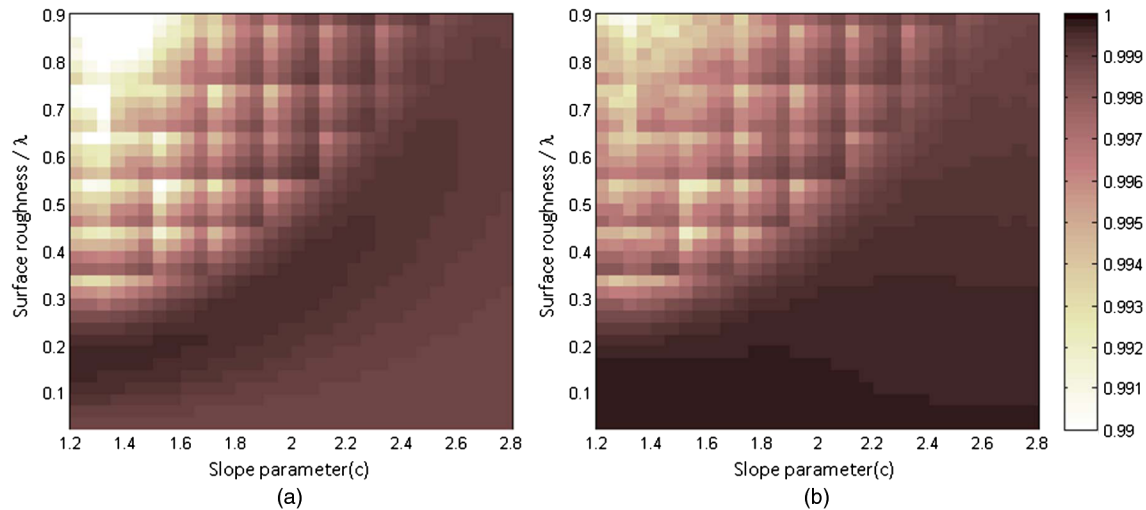


Fig. 19 Total reflected energy using the MoM for 36×36 cases of the surface parameter sets $(c, \hat{\sigma}_{\text{tot}})$ for (a) $\theta_i = 0$ deg and (b) $\theta_i = 60$ deg.

frequency of the surface is smaller than the shoulder frequency. Regarding the number of the sampling points per wavelength, eight points to 50 points per wavelength are used for different surface parameter sets. Each number is obtained by comparing the MoM prediction to another MoM prediction with a different $\lambda/\Delta x$ value. The idea is that, if the $\lambda/\Delta x$ value is large enough for the MoM simulation, the simulation results are not changed significantly when comparing it to another MoM simulation with much larger $\lambda/\Delta x$ values.^{20,35} In our simulation, the “large enough” $\lambda/\Delta x$ values depend on the rms roughness and the slope parameter and, specifically, the case of a smaller c value and larger rms roughness requires a larger value of “large enough” $\lambda/\Delta x$ value. Fixing $b = 20$, we divided the surface parameter space into 91 subspaces and obtained the “large enough” $\lambda/\Delta x$ values for each subspace and they are shown in Fig. 18.

Using the selected $\lambda/\Delta x$ values in Fig. 18, the total fractional reflected energy for 36×36 cases of the surface parameter sets are calculated and shown in Fig. 19. Figure 19(a) is for the case of normal incidence and Fig. 19(b) is for the case of 60 deg of the incident angle. In our simulation, the total fractional reflected energy predicted by the MoM drops by 1% in the region of large rms roughness and small slope parameter value. However, in most of the domain of interest, the energy conservation condition is almost satisfied for our MoM simulations.

6 Conclusion

In this paper, the valid domains of the three approximate methods are evaluated by numerical comparison to the rigorous MoM for 1-D perfectly conducting random rough surfaces having Gaussian and abc -function surface PSDs. The relative accuracy of the three approximate methods has been calculated and graphically illustrated over the domain of interest in terms of the rms roughness and surface correlation length for surfaces with a Gaussian surface PSD and in terms of the rms roughness and the slope parameter for surfaces with an abc -function surface PSD. Regarding the region of validity for surfaces with a Gaussian statistics, the SPM shows a good agreement in the smooth surface regime, and its accuracy depends upon both smoothness and

correlation length. Our analysis shows that the valid domain of the KA method depends largely on the rms slope rather than rms curvature of the random surface and the accuracy of its prediction increases almost linearly with an increasing surface correlation length. In general, numerical comparison also reveals that the GHS method has a much broader domain of validity than the other two approximate methods, and it is shown that the valid domain depends on the rms slope of the surface. When it comes to valid domains of those approximate methods for surfaces with abc -function surface PSD, the SPM shows a good agreement for the surface with the small rms roughness. Surprisingly, the SPM accurately predicts scattering behavior at the large scattering angles not only for smooth surfaces, but also for moderately rough surfaces which do not satisfy the smooth surface criterion. The KA fails to predict scattering behavior at the large scattering angles but it shows accurate predictions near the specular direction for surfaces whose ratio of the rms roughness to the slope parameter c is small. The GHS theory shows quite accurate scattering predictions from smooth to quite rough surfaces over almost all scattering angles. Similar to the case of the KA, its region of validity depends on the ratio of the rms roughness to the slope parameter c , but the valid region is much wider than for the KA and SPM theories. Moreover, it has high accuracy not only for small incident angles but also for relatively large angles of incidence. The energy conservation condition is investigated for the MoM results in order to show its reliability as a rigorous reference to the other methods. Our result is obtained from 1-D TE cases, thus it would be quite interesting to investigate that this trend of the validity holds for 2-D surfaces.

References

1. T. M. Elfouhaily and C. A. Guerin, “A critical survey of approximate scattering wave theories from random rough surfaces,” *Waves Random Media* **14**(4), R1–R40 (2004).
2. S. O. Rice, “Reflection of electromagnetic waves from slightly rough surfaces,” *Commun. Pure Appl. Math.* **4**(2–3), 351–378 (1951).
3. P. Beckmann and A. Spizzichino, *The Scattering of Electromagnetic Waves from Rough Surfaces*, Pergamon Press, New York (1963).
4. A. Krywonos, J. E. Harvey, and N. Choi, “Linear systems formulation of surface scatter theory for rough surfaces with arbitrary incident and scattering angles,” *J. Opt. Soc. Am. A* **28**(6), 1121–1138 (2011).

5. J. E. Harvey et al., “Diffracted radiance: a fundamental quantity in a non-paraxial scalar diffraction theory,” *Appl. Opt.* **38**(31), 6469–6481 (1999).
6. J. E. Harvey et al., “Diffracted radiance: a fundamental quantity in a non-paraxial scalar diffraction theory: errata,” *Appl. Opt.* **39**(34), 6374–6375 (2000).
7. K. F. Warnick and W. C. Chew, “Numerical simulation methods for rough surface scattering,” *Waves Random Media* **11**(1), R1–R30 (2001).
8. N. Garcia and E. Stoll, “Monte Carlo calculation for electromagnetic-wave scattering from random rough surfaces,” *Phys. Rev. Lett.* **52**(20), 1798–1801 (1984).
9. E. Thorsos, “The validity of the Kirchhoff approximation for rough surface scattering using a Gaussian roughness spectrum,” *J. Acoust. Soc. Am.* **83**(1), 78–92 (1988).
10. S. L. Broschat, E. I. Thorsos, and A. Ishimaru, “The phase perturbation technique vs. an exact numerical method for random rough surface scattering,” *J. Electromagnet. Wave* **3**(3), 237–256 (1989).
11. E. Thorsos and D. R. Jackson, “The validity of the perturbation approximation for rough surface scattering using a Gaussian roughness spectrum,” *J. Acoust. Soc. Am.* **86**(1), 261–277 (1989).
12. J. M. Soto-Crespo and M. Nieto-Vesperinas, “Electromagnetic scattering from very rough random surfaces and deep reflection gratings,” *J. Opt. Soc. Am. A* **6**(3), 367–384 (1989).
13. J. M. Soto-Crespo, M. Nieto-Vesperinas, and A. T. Friberg, “Scattering from slightly rough random surfaces: a detailed study on the validity of the small perturbation method,” *J. Opt. Soc. Am. A* **7**(7), 1185–1201 (1990).
14. E. I. Thorsos and D. R. Jackson, “Studies of scattering theory using numerical methods,” *Waves Random Media* **1**(3), 165–190 (1991).
15. Y. Kuga, C. T. C. Le, and A. Ishimaru, “Analytical, experimental, and numerical studies of angular memory signatures of waves scattered from one-dimensional rough surfaces,” *IEEE Trans. Geosci. Remote Sens.* **34**(6), 1300–1307 (1996).
16. S. L. Broschat and E. I. Thorsos, “An investigation of the small slope approximation for scattering from rough surfaces. Part II. Numerical studies,” *J. Acoust. Soc. Am.* **101**(5), 2615–2625 (1997).
17. J. A. Sánchez-Gil and M. Nieto-Vesperinas, “Light scattering from random rough dielectric surfaces,” *J. Opt. Soc. Am. A* **8**(8), 1270–1286 (1991).
18. J. T. Johnson et al., “A numerical study of the composite surface model for ocean backscattering,” *IEEE Trans. Geosci. Remote Sens.* **36**(1), 72–83 (1998).
19. J. M. Sturm and J. C. West, “Numerical study of shadowing in electromagnetic scattering from rough dielectric surfaces,” *IEEE Trans. Geosci. Remote Sens.* **36**(5), 1477–1484 (1998).
20. G. Franceschetti, A. Iodice, and D. Riccio, “Scattering from dielectric random fractal surfaces via method of moments,” *IEEE Trans. Geosci. Remote Sens.* **38**(4), 1644–1655 (2000).
21. J. V. Toporkov and G. S. Brown, “Numerical study of the extended Kirchhoff approach and the lowest order small slope approximation for scattering from ocean-like surfaces: Doppler analysis,” *IEEE Trans. Antennas Propag.* **50**(4), 417–425 (2002).
22. Q. Li, C. H. Chan, and L. Tsang, “Monte Carlo simulations of wave scattering from lossy dielectric random rough surfaces using the physics-based two-grid method and the canonical-grid method,” *IEEE Trans. Antennas Propag.* **47**(4), 752–763 (1999).
23. K. Pak et al., “Backscattering enhancement of electromagnetic waves from two-dimensional perfectly conducting random rough surfaces based on Monte Carlo simulations,” *J. Opt. Soc. Am. A* **12**(11), 2491–2499 (1995).
24. I. Simonsen, A. A. Maradudin, and T. A. Leskova, “Scattering of electromagnetic waves from two-dimensional randomly rough perfectly conducting surfaces: The full angular intensity distribution,” *Phys. Rev. A* **81**(1), 013806 (2010).
25. I. Simonsen, A. A. Maradudin, and T. A. Leskova, “Scattering of electromagnetic waves from two-dimensional randomly rough penetrable surfaces,” *Phys. Rev. Lett.* **104**(22), 223904 (2010).
26. K. A. O’Donnell and E. R. Mendez, “Experimental study of scattering from characterized random surfaces,” *J. Opt. Soc. Am. A* **4**(7), 1194–1205 (1987).
27. E. L. Church, “Fractal surface finish,” *Appl. Opt.* **27**(8), 1518–1526 (1988).
28. R. J. Noll and P. Glenn, “Mirror surface autocovariance functions and their associated visible scattering,” *Appl. Opt.* **21**(10), 1824–1838 (1982).
29. J. E. Harvey, “Light-scattering characteristics of optical surfaces,” Ph.D. Dissertation, University of Arizona (1976).
30. J. C. Stover, *Optical Scattering, Measurement and Analysis*, 2nd ed., SPIE Press, Bellingham, WA (1995).
31. R. T. Austin, A. W. England, and G. H. Wakefield, “Special problems in the estimation of power-law spectra as applied to topographical modeling,” *IEEE Trans. Remote Sens.* **32**(4), 928–939 (1994).
32. C. Guérin and M. Saillard, “Electromagnetic scattering on fractional Brownian surfaces and estimation of the Hurst exponent,” *Inverse Prob.* **17**(3), 365–386 (2001).
33. G. Franceschetti et al., “Scattering from natural rough surfaces modeled by fractional Brownian motion two-dimensional Processes,” *IEEE Trans. Geosci. Remote Sens.* **38**(4), 1405–1415 (2000).
34. L. Tsang et al., *Scattering of Electromagnetic Waves: Numerical Simulations*, pp. 132–134, Wiley, New York (2001).
35. A. K. Sultan-Salem and G. L. Tyler, “Validity of the Kirchhoff approximation for electromagnetic wave scattering from fractal surfaces,” *IEEE Trans. Geosci. Remote Sens.* **42**(9), 1860–1870 (2004).
36. J. M. Elson, J. M. Bennett, and J. C. Stover, “Wavelength and angular dependence of light scattering from beryllium: comparison of theory and experiment,” *Appl. Opt.* **32**(19), 3362–3376 (1993).



analysis of optical systems and optical system integration.

Narak Choi received a bachelor’s degree in physics from Seoul National University in 2007, and a PhD degree in optics from the College of Optics and Photonics at the University of Central Florida in 2012. He is credited with approximately 20 publications and conference presentations in the areas optical design and analysis and image degradation due to surface scatter phenomena. He is currently working for Photonic Systems Integrated, LLC, in the area of optical design,



James E. Harvey is a retired associate professor from CREOL: the College of Optics and Photonics at the University of Central Florida, and currently a senior optical engineer with Photon Engineering, LLC in Tucson AZ. He has a PhD in optical sciences from the University of Arizona and is credited with over 200 publications and conference presentations in the areas of diffraction theory, surface scatter phenomena, adaptive optics, wavefront sensing, beam sampling technology, optical properties of materials, phased telescope arrays, and x-ray/EUV imaging systems. He is a member of OSA and a Fellow and past board member of SPIE.